

学位論文（要約）

**Analyses on mechanisms that establish the nine-fold symmetry of
the centriole using protein engineering approaches**

（タンパク質改変による中心子9回対称性構造の確立機構の解析）

平成29年12月博士（理学）申請

東京大学大学院理学系研究科

生物科学専攻

苗加 彰

Doctoral Dissertation

**Analyses on mechanisms that establish the nine-fold symmetry of
the centriole using protein engineering approaches**

Doctoral Dissertation

Submitted to the Graduate School of Science, University of Tokyo

Akira Noga

December, 2017

CONTENTS

Abbreviations.....	1
General Introduction.....	2
Part I Engineering of SAS-6 reveals interdependence between the cartwheel and microtubules in establishing the nine-fold symmetry of the centriole	
Abstract.....	11
Introduction.....	12
Material and methods.....	14
Results.....	19
Discussion.....	35
Part II	
5年以内に雑誌等で刊行予定のため、非公開。	
Abstract.....	40
Introduction.....	41
Material and methods.....	43
Results.....	47
Discussion.....	64
General Discussion.....	68
Acknowledgements.....	71
References.....	72

Abbreviations

AFM	atomic force microscopy
DTT	dithiothreitol
EM	electron microscopy
FITC	fluorescein isothiocyanate
HA	haemagglutinin
HRP	horseradish peroxidase
IgG	immunoglobulin G
IPTG	isopropyl- β -D-thiogalactopyranoside
Kd	dissociation constant
MTOC	microtubule organizing center
NFAp	nucleoflagellar apparatus
PBS	phosphate buffered saline
PCM	pericentriolar material
PCR	polymerase chain reaction
SDS-PAGE	sodium dodecyl sulfate-polyacrylamide gel electrophoresis
STAN	<u>STIL</u> / <u>Ana2</u>
TAP	tris acetate phosphate
TIM	truncated in microcephaly

General Introduction

The centriole is a cell organelle that plays a central role in the assembly of microtubule cytoskeletons, serving as the core of the centrosome and as the basal structure of cilia and flagella (Fig. 1).

The centrosome, which consists of a pair of centrioles and the pericentriolar material (PCM) surrounding the centrioles, functions as the microtubule-organizing center (MTOC) in most animal cells (Fig. 1B; Conduit, Wainman, and Raff 2015; Bornens 2012). During interphase, the centrosome located near the nucleus organizes cytoplasmic microtubules into a radial array, which serves as the track for intracellular transport driven by kinesin and dynein. During mitosis, duplicated centrosomes, together with the radial microtubule arrays, form a bipolar spindle for chromosome segregation. In reflection of these crucial roles of the centrosome in mitosis, many mutations of centrosomal proteins are associated with various serious diseases such as cancer and primary microcephaly (Nigg and Raff 2009; Bettencourt-Dias et al. 2011).

Cilia are hair-like organelles that protrude from the cell. Motile cilia and flagella produce fluid flow by periodic bending movement, while immotile cilia function as cellular antennas that detect various external signals. Because of these important functions, mutations affecting the ciliary assembly or function lead to “ciliopathies”, which include hydrocephalus, situs inversus, and polycystic kidney disease in mice and humans. The inner core of cilia, called the axoneme, contains 9 doublet microtubules grown from centriole microtubules (Fig. 1). The centriole serving as the base for the axoneme assembly has another name, “the basal body”.

The centriole is assembled through a semi-conservative duplication process that occurs once per cell cycle. In animal cells, a nascent centriole starts to assemble on the sidewall of the pre-existing centriole at the G1/S phase, and develops until the G2 phase (Kuriyama and Borisy 1981; Firat-Karalar and Stearns 2014). The new and old centrioles separate immediately after mitosis. This separation, called “disengagement”, allows the assembly of new centrioles of next generation. This assembly process, depending on the pre-existing centriole, appears important for maintaining the proper number of centrioles in the cell throughout the cell cycle.

The centriole has a cylindrical structure consisting of 9 triplet microtubules arranged in a rotational symmetry (Fig. 2A; Winey and O'Toole 2014). When it functions as the basal body, 9 triplet microtubules serve as the template of the 9 doublet microtubules of the axoneme (Fig. 2B). Thus, the centriole's architecture defines the structural pattern of the axoneme. Strikingly, these characteristic structures of the centriole and the axoneme with 9 microtubules are highly conserved among almost all eukaryotic organisms. This fact strongly suggests that the common ancestor of all eukaryotes already had a 9-fold symmetrical centriole. Why is the 9-fold symmetry highly conserved throughout eukaryotic evolution? What mechanisms establish the 9-fold symmetry? Many scientists have had these questions since the structures of cilia and centrioles were observed by electron microscopy (EM) in 1950s (Fawcett and Porter 1954; de Harven and Bernhard 1956). However, no clues to these questions were obtained until recently.

The first clues to the latter question came from the analyses of a *Chlamydomonas* mutant, *bld10* (Matsuura et al. 2004). *Chlamydomonas*, a

biflagellated green alga, is a model organism that has been extensively used in genetic and biochemical studies of flagellar assembly and motility. The *blid10* mutant, totally lacking the centriole and flagella, has a null mutation in the gene coding for Bld10p, a coiled-coil protein homologous to a mammalian centrosomal protein Cep135. An interesting finding relevant to the centriolar 9-fold symmetry is its localization. It is localized to the cartwheel, a 9-fold symmetrical structure that consists of the central hub and 9 spokes and is located in the lumen of the centriole. In the assembly process of the centriole, it appears in an early stage when the centriole's 9-fold symmetry establishes. These observations led to a hypothesis that it functions as the scaffold for the assembly of centriolar microtubules. However, no clues had been obtained as to the cartwheel's function.

To investigate the function of Bld10p in the cartwheel, Hiraki et al. (2007) constructed *blid10* strains expressing a series of truncated Bld10ps. Interestingly, the expression of such short Bld10ps as the construct $\Delta N3$, which lacks the N-terminal 53% of the amino acid sequence, and $\Delta C2$, which lacks the C-terminal 35%, partially rescue the flagella-less phenotype of *blid10*. In these strains, the centrioles have cartwheels with shorter spokes, and connections between centriolar microtubules and the cartwheel spokes are often broken. Most interestingly, centrioles in these strains often have 8 triplet microtubules while their cartwheels have 9 spokes. These findings suggest that the proper spoke length, and the interaction between the centriolar microtubules and the cartwheel spokes are important for stabilizing the 9-fold centriole symmetry. This was the first experimental evidence for the importance of the cartwheel in the establishment of 9-fold symmetry.

The importance of the cartwheel was further supported by analyses of

another *Chlamydomonas* mutant, *bld12* (Nakazawa et al. 2007). This mutant has a null mutation in the gene for SAS-6, a centrosomal protein highly conserved among organisms that have centrioles. EM observations of the *bld12* centriole revealed that SAS-6 constitutes the central part of the cartwheel, namely, the hub and the 9 radially-arranged spokes. Interestingly, the centrioles without the central part have variable numbers of triplet microtubules ranging from 7 to 11. This finding clearly shows that the cartwheel is required for fixing the number of the triplets to 9.

X-ray crystallography and biochemical analyses of SAS-6 provided information about how this molecule assembles into the radial part of the cartwheel structure (Kitagawa et al. 2011; van Breugel et al. 2011). SAS-6 consists of an N-terminal domain, a coiled-coil domain, and a C-terminal domain, and forms a parallel homodimer via association of the coiled-coil domains. The dimer, which has two globular heads (corresponding to the N-terminal domain) and a rod-shaped coiled-coil tail (the coiled-coil domain), self-assembles in vitro into a cartwheel-like structure through interaction between the heads. As revealed by the expression of mutated SAS-6s in *bld12*, the self-assembling property is essential for the SAS-6 function in the formation of the centriole. These findings suggest that the central part of the cartwheel is composed of 9 SAS-6 dimers.

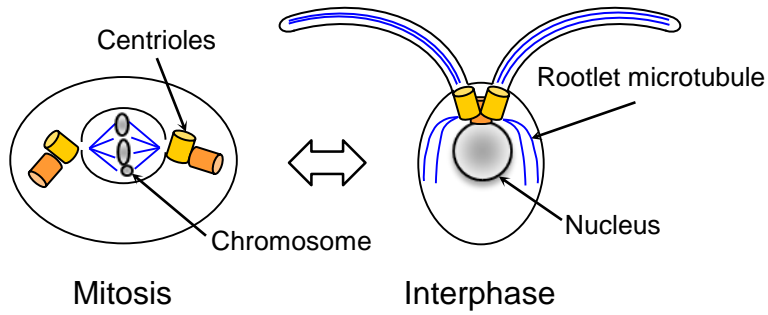
These findings have led to a speculation that the self-assembling property of SAS-6 determines the conserved 9-fold symmetrical structure of the centriole, through formation of the cartwheel that nucleates centriolar microtubules (Gonczy 2012; Hirono 2014; Loncarek and Bettencourt-Dias 2017). However, the fact that the majority of the centrioles in *bld12* have 9 triplet microtubules is

obviously inconsistent with this speculation, and suggests that another mechanism, independent of SAS-6 and the cartwheel, also contributes to the establishment of 9-fold symmetry (Fig. 3; Nakazawa et al. 2007). Thus, the phenotype of the *bld12* mutant raises new questions as to whether there actually is a cartwheel-independent mechanism for the determination of 9-fold symmetry, and if it does exist, what molecules function in that mechanism and how it cooperates with the cartwheel-dependent mechanism.

To address these questions, in Part I, I attempted to change the degree of rotational symmetry of the cartwheel by expressing genetically engineered SAS-6s in *bld12*, and examined their effects on the centriole structure. The results suggest a possibility that the 9-fold symmetry of the centriole is established through a dynamic interaction between the cartwheel and the microtubule wall that is assembled independently of the cartwheel. In Part II,

5年以内に雑誌等で刊行予定のため、非公開。

A



B

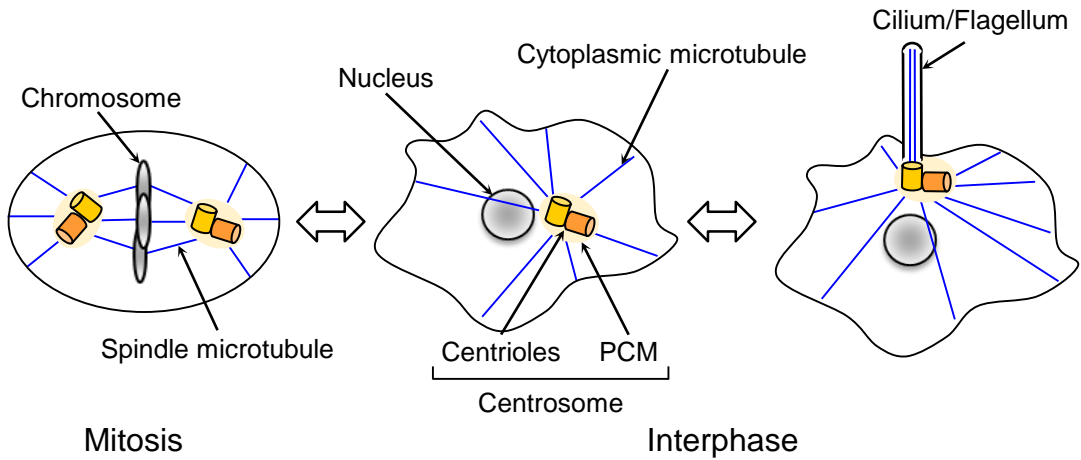


Figure 1. Dual function of the centriole

Schematic localization of centrioles in *Chlamydomonas* (A) and animal cells (B). The centriole functions as the core of the centrosome and as the base of cilium.

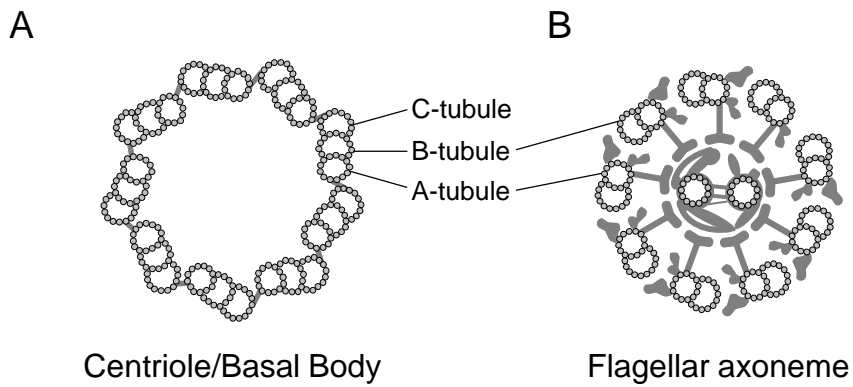


Figure 2. Structures of the centriole (A) and ciliary axoneme (B)

The centriole consists of 9 triplet microtubules arranged in rotational symmetry. The triplet microtubule consists of 3 tubules called A-, B-, and C-tubules. Of these, A- and B-tubules serve as the templates of the A- and B-tubules of the doublet microtubule of the axoneme.

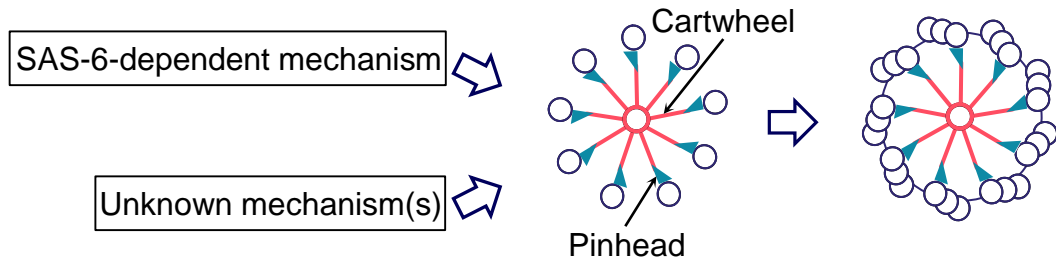


Figure 3. Mechanisms that establish the 9-fold symmetry of the centriole
 During establishment of the 9-fold symmetry, not only the mechanism dependent on the self-association of SAS-6 but also unknown cartwheel-independent mechanism(s) should be important. In the proximal lumen of the centriole, the cartwheel (pink) is located. A bulge that connects the cartwheel and the triplet microtubule is the pinhead (light blue).

Part I

**Engineering of SAS-6 reveals interdependence
between the cartwheel and microtubules
in establishing the nine-fold symmetry of the centriole**

Abstract

Centrioles have a conserved cylindrical structure with 9 triplet microtubules arranged in rotational symmetry. Analyses of *Chlamydomonas bld12* (a null mutant of SAS-6) have shown the critical importance of the cartwheel for the establishment of the 9-fold symmetrical centriole structure. However, the formation of this structure is suggested to depend on factors other than the cartwheel also. To understand the precise role of the cartwheel in centriole assembly, I produced a series of mutated SAS-6 proteins that assemble in vitro into cartwheel-like structures with 5- to 10-fold symmetries, and expressed them in *bld12*, a *Chlamydomonas* mutant that has a null mutation in the SAS-6 gene. Unexpectedly, a mutated SAS-6 that preferentially formed a 6-fold symmetrical structure in vitro, frequently produced 9-fold symmetrical cartwheels and centrioles in vivo. However, when it was expressed in combination with a truncated Bld10p, which caused weakened connection between the cartwheel spokes and triplet microtubules, 6- to 8-fold symmetrical cartwheels and 8- to 9-fold symmetrical centrioles were formed in vivo. These results suggest that the centriolar microtubules have an intrinsic ability to assemble into cylindrical structures with an ~9-fold symmetry, and that the assembled microtubule wall affects the symmetry of the cartwheel. I surmise that cartwheels and microtubules assemble independently of each other, and their interaction stabilizes only the centrioles with 9-fold symmetry. The formation of the correct centriole structure may thus involve a hitherto unrecognized dynamic process.

Introduction

Centrioles have a conserved structure consisting of 9 triplet microtubules (Fig. 2A). This structural pattern with 9-fold symmetry is highly conserved among eukaryotes. Recent studies using a *Chlamydomonas* mutant, *bld12*, showed that the cartwheel, a sub-centriolar structure that appears at an early stage of centriole assembly process, is critically important for establishing the 9-fold symmetry of the centriole structure. The cartwheel consists of the central hub and 9 spokes extending from the hub. The *bld12* mutant lacks the central part of the cartwheel, and, interestingly, produces centrioles with variable numbers of triplet microtubules ranging from 7 to 11. These observations indicate that the cartwheel has a crucial role for stabilizing the number of the centriolar microtubules to 9 (Nakazawa et al. 2007).

bld12 has a null mutation in the gene for SAS-6, a conserved centriole protein. X-ray crystallography and biochemical analyses revealed that SAS-6 forms a dimer with two globular heads and a rod-shaped tail via association of the coiled-coil domains (Kitagawa et al. 2011; van Breugel et al. 2011). Intriguingly, this dimer preferentially self-assembles into a cartwheel-like structures with 8- or 9-fold symmetry in vitro. Mutational analyses of SAS-6 and immuno-electron microscopy using *bld12* showed that the self-association property of SAS-6 is crucial for in vivo assembly of the cartwheel, and that the SAS-6 dimer in the cartwheel is positioned in vivo in the same direction as in vitro. These results strongly suggest that the cartwheel consists of 9 SAS-6 dimers assembled through self-association.

These findings have led to a speculation that the ability of SAS-6 to form

a 9-fold symmetrical structure in vitro determines the 9-fold symmetry of the centriole. In fact, this hypothesis is widely accepted (Gonczy 2012; Hirono 2014; Loncarek and Bettencourt-Dias 2017). However, it must be noted that, despite the lack of the cartwheel in *bld12*, 70% of the centriole images have normal-shaped centrioles with 9-fold symmetry (Nakazawa et al. 2007). This observation suggests that not only the mechanism dependent on the cartwheel but also another mechanism independent of SAS-6 contributes to establishing the 9-fold symmetry of the centriole (Fig. 3). However, the entity of the cartwheel-independent mechanism, as well as how this mechanism is related to the cartwheel-dependent mechanism, is not understood.

To address these problems, I examined the centriole structure in cells that were forced to produce cartwheels with altered rotational symmetry by expression of engineered SAS-6 genes. The results suggest that the cartwheel and the centriolar triplet microtubules assemble independently, and that the dynamic interaction between them establishes the 9-fold symmetry of the centriole.

Material and methods

Protein production and purification

Chlamydomonas SAS-6 (Uniprot ID A9CQL4) N-terminal domain variants (residues 1-159), named NN SAS-6s, were generated by PCR mutagenesis (Olieric et al. 2010) and verified by Sanger sequencing.

For protein production, expression plasmids were transformed into the *E. coli* strain BL21 (DE3) (Stratagene). 4-6 liters of LB media supplemented with 50 µg/mL kanamycin were inoculated with an O/N culture. After incubation for 4h at 37°C, protein expression was induced at an OD₆₀₀ of 0.6 by the addition of 0.4 mM isopropyl 1-thio-β-galactopyranoside (IPTG) over night at 20 °C.

Cell pellets were lysed by lysozyme treatment and sonication, resuspended in lysis buffer containing 50 mM Tris-HCl, pH 7.5, 500 mM NaCl, 10mM imidazole, complete protease inhibitor (Roche) and 5 mM β-mercaptoethanol. Cell debris were removed by centrifugation. Supernatants were applied onto a HistTrap crude FF immobilized metal-affinity column (IMAC) (loading buffer: 50 mM Tris-HCl, pH 7.5, 500 mM NaCl, 10mM imidazole, 5 mM β-mercaptoethanol; washing buffer: same but containing 70 mM imidazole; elution buffer: same but containing 200 mM imidazole). Eluted proteins were further purified on a Superdex S200 16/60 size exclusion column (SEC buffer: 50 mM Tris-HCl, pH 7.5, 150 mM NaCl, 5 mM β-mercaptoethanol) according to the manufacturer's instructions (GE Healthcare).

Proteins used for AFM imaging were incubated in 20 mM Tris-HCl, pH 7.4, 150 mM NaCl, 2.5 mM CaCl₂ over night at 4 °C with thrombin (Sigma

Aldrich) to remove the 6xHis-tag after the first IMAC. Processed proteins were separated from the cleaved His-tags by a second IMAC chromatography step prior to the final size exclusion chromatography step.

Measurements of dissociation constants

Isothermal titration calorimetry (ITC) experiments were performed at 10 °C with an ITC200 calorimeter (Microcal). SAS-6 N-terminal domain samples in the syringe (0.6-1.6 mM) were injected stepwise into SEC buffer. The dissociation isotherms were fitted using a nonlinear least squares minimization method provided with the calorimeter.

Atomic force microscopy (AFM)

SAS-6 N-CC protein samples were diluted in adsorption buffer (300 mM KCl, 20 mM Tris-HCl, pH 7.2) to reach a final concentration of 5 μ M. Thirty microliter of sample were adsorbed for 10 min onto a freshly cleaved mica surface. The samples were subsequently rinsed 5 times with imaging buffer (20 mM Tris-HCl, pH 7.2, 150 mM KCl) and characterized by AFM in imaging buffer and at room temperature (26°C) as described (Pfreundschuh et al. 2014). Briefly, the AFM (Multimode 8 equipped with a Nanoscope V controller, Bruker, Santa Barbara, California, USA) was operated in the 'PeakForceTapping' mode. The AFM was equipped with a 120 μ m piezoelectric scanner. Rectangular Si₃N₄ cantilevers having a nominal spring constant of \approx 0.04-0.08 N/m and a resonance frequency in water of \approx 35 kHz were chosen (Biolever Mini, Olympus). AFM topographs (frame size 0.5-3 μ m) were recorded applying a vertical oscillation frequency of 2 kHz

and amplitude of 25 nm to the AFM cantilever, an imaging force of 45-65 pN, a scanning frequency of 0.3-0.8 line/second, and recording topographs of 512x512 or 1024x1024 pixels in size.

***Chlamydomonas* strains**

The *Chlamydomonas* wild-type strain CC124 and the cell-wall-less mutant *cw92* were obtained from the *Chlamydomonas* Resource center (University of Minnesota, St. Paul, MN). The mutant *bld12-1* (referred to as *bld12* in this paper) has been previously described (Nakazawa et al. 2007). *bld12* strains expressing the wild type SAS-6 tagged with HA, and *bld10* strains expressing truncated Bld10ps (*bld10::ΔC2* and *bld10::ΔN3*) have been described elsewhere (Matsuura et al. 2004; Hiraki et al. 2007; Nakazawa et al. 2007), but these expression strains were reestablished. *bld10bld12::NN24ΔC2*, and *bld10bld12::NN24ΔN3* were produced using standard methods of genetic cross. Cells were grown in Tris-acetate-phosphate (TAP) medium (Gorman and Levine 1965) with aeration on a 12hr/12hr light/dark cycle, or under constant illumination with agitation.

Establishment of *bld12* strains expressing engineered SAS-6s

A genomic fragment containing the SAS-6 gene was cloned in pBluescript KS(+). The mutations for the four NN SAS-6s were introduced into the fragment by overlap extension PCR. The plasmids were digested with Bsp1407I, and 1.3-kb fragments containing the mutagenized sequences were subcloned in the original plasmid digested with Bsp1407I to replace the corresponding fragments. The sequences of the replaced region were verified by Sanger sequencing. Each

plasmid was mixed with another plasmid, pSI103, carrying the selectable marker gene *aphVIII* (Sizova, Fuhrmann, and Hegemann 2001), and introduced into *bld12* by electroporation (Shimogawara et al. 1998). The cells were cultivated on TAP agar plates containing 10 µg/ml paromomycin. For each strain, about 500 colonies forming on the agar plates were isolated and subjected to western blot using anti-HA antibody. A clone expressing the engineered SAS-6 most efficiently was used for the experiments.

Western blot analyses

Whole-cell extracts (10 µg/lane) were separated by SDS-PAGE and transferred to Immobilon-P membranes (Millipore). An affinity-purified rabbit polyclonal antibody against SAS-6 (Nakazawa et al. 2007) (1/1000), a Rat monoclonal antibody against HA (clone 3F10, Roche) (1/2000), a rabbit antibody against the 120 N-terminal residues of Bld10p (Hiraki et al. 2007) (1/200), and a rabbit antibody against the C-terminal one-third of Bld10p (Matsuura et al. 2004) (1/500) were used as primary antibodies. A goat anti-rabbit-IgG conjugated Horseradish Peroxidase (Sigma-Aldrich) (1/2000) and a goat anti-rat-IgG conjugated Horseradish Peroxidase (Sigma-Aldrich) (1/3000) were used as secondary antibodies.

Immunofluorescence microscopy

Chlamydomonas cells grown in liquid medium were attached onto a glass slide coated with 0.1% polyethylenimine. The cells were fixed for 10 min in -20°C methanol, washed 3 times in PBS, and incubated with a blocking solution (10

mM sodium phosphate buffer pH 7.2, 5% normal goat serum, 5% glycerol, 1% fish gelatin, 0.004% sodium azide) for 30 min at 37°C. The fixed cells were incubated for 1 hr at 37°C with primary antibodies, rat monoclonal antibody against HA (clone 3F10, Roche) and anti-acetylated α -tubulin (monoclonal 6-11B-1, Sigma-Aldrich) both diluted to 1:100 in blocking solution, and washed three times for 15 min in PBS. The cells were stained for 1 hr at 37°C with secondary antibodies, goat anti-rat IgG coupled to Alexa594 (Sigma-Aldrich) and goat anti-mouse IgG coupled to FITC (Sigma-Aldrich) diluted in blocking solution to 1:200, and washed three times for 15 min in PBS. Images were recorded using an Axioplan fluorescence microscope (Carl Zeiss MicroImaging) with a 63 \times 1.4 NA plan-APOCHROMAT objective and a CoolSNAP CCD camera (Roper Scientific).

Counting flagellated cells

Log-phase cells were treated with gametic autolysin (Harris 1989) to remove the cell wall and induce flagellar growth. The cells were fixed with 1% glutaraldehyde and observed under a dark-field microscope. Percentages of flagellated cells were determined by counting cells with two, one, and zero flagella.

Electron microscopy (EM)

Nucleo-flagellar apparatus (NFAP), a cytoskeletal complex that contains centrioles, was isolated from *Chlamydomonas* cells as described Wright et al. (1985). The NFAP was prefixed with 2% glutaraldehyde and 1% tannic acids in 50 mM sodium phosphate buffer (pH 7.2) for 1 hr at 0°C, and postfixated with 1%

OsO₄ in phosphate buffer for 1 hr. The samples were dehydrated and embedded in EPON 812 resin. Thin sections 70-nm thick were stained with 7% uranyl acetate and Reynolds' lead citrate, and observed under a transmission EM.

Results

In vitro self-assembly properties of engineered SAS-6s

Recombinant *Chlamydomonas* SAS-6 containing the N-terminal domain and the coiled-coil domain forms dimers, and the dimers self-assemble into cartwheel-like oligomers *in vitro* through a weak head-to-head interaction. In collaboration with Dr. Steinmetz's group at Paul Scherrer Institute, Switzerland, I produced 28 variants of recombinant SAS-6 with reinforced head-to-head interaction between dimers, by introducing mutations into the N-terminal domain. These mutations reduced the dissociation constants (Kd) of the proteins by 1-3 orders of magnitude (Table 1). The engineered proteins were named NN1 to NN28 (NN stands for "between two N-terminal domains").

The SAS-6 variants with NN2, NN15, NN24, or NN26 mutations displayed clearly different self-assembly properties from that of the wild-type SAS-6. The wild-type SAS-6 assembled into 9-dimer cartwheel-like structures most frequently, although the number of dimers varied from 8 to 10 (Table 1, Fig. 4). In contrast, the SAS-6 protein with NN2 or NN15 mutation assembled into 8-dimer structures, and that with NN24 mutation assembled into 6-dimer structures most frequently. The protein with NN26 mutation assembled into 8-dimer structure, while its dissociation constant was almost the same as that of NN24 (Table 1, Fig. 4).

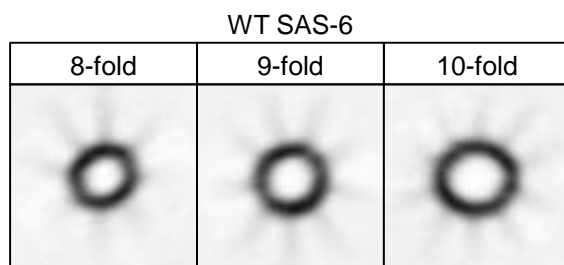
Establishment of *Chlamydomonas* strains expressing engineered SAS-6s

To examine *in vivo* effects of NN2, NN15, NN24, and NN26 mutations, *Chlamydomonas* strains expressing each of these engineered SAS-6s were

Name	Mutations	Kd μM	Symmetry
WT SAS-6	-	350±30	8, 9, 10 (31%, 43%, 27%)
SAS-6 with NN2 mutation	F145W	78±4	7, 8, 9 (28%, 40%, 31%)
SAS-6 with NN15 mutations	G94D Q147R	20.3±0.1	8, 9, 10 (47%, 46%, 7%)
SAS-6 with NN24 mutations	Q93E F145W K146R	2.3±0.1	5, 6, 7 (20%, 65%, 16%)
SAS-6 with NN26 mutations	G94E F145W Q147K	4±3	7, 8, 9 (32%, 49%, 19%)

Table 1. In vitro properties of engineered SAS-6s used in this study

A



B

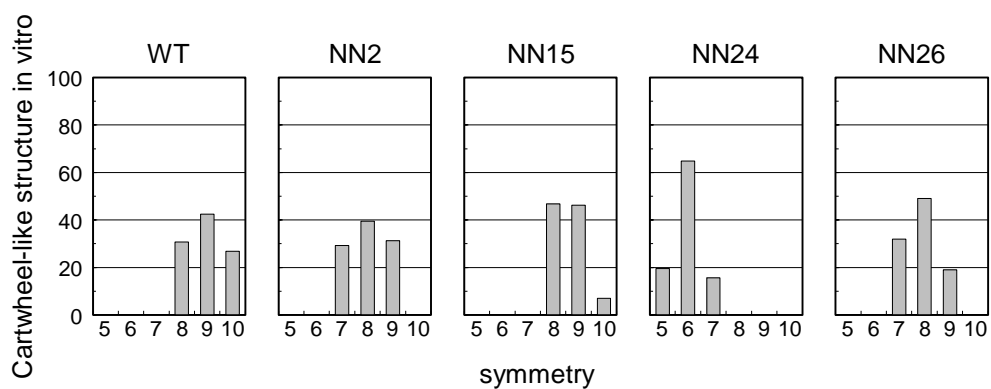


Figure 4. Engineered SAS-6s preferentially assembled with the smaller numbers of dimers in vitro

(A) AFM topographs of the wild type SAS-6. (B) Determination of in vitro symmetries of wild type SAS-6, NN2, NN15, NN24 and NN26.

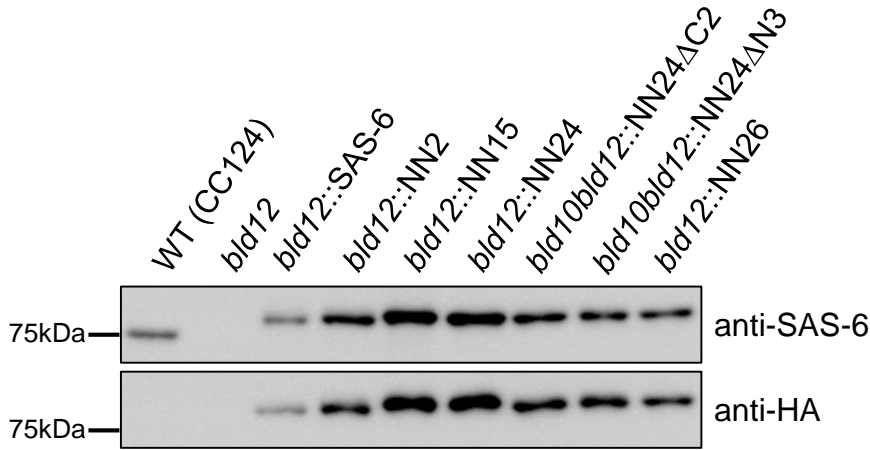
produced. Plasmid constructs containing the engineered SAS-6 genes C-terminally tagged with 3xHA were introduced into *bld12-1*, a mutant that totally lacks the SAS-6 gene (Nakazawa et al. 2007). Hereafter, engineered SAS-6 proteins carrying these NN mutations are referred to as NN2, NN15, NN24, NN26, and the *bld12* strains expressing wild type SAS-6 and engineered SAS-6s are referred to as *bld12::SAS-6*, *bld12::NN2*, *bld12::NN15*, *bld12::NN24*, and *bld12::NN26*. Western blot analysis showed that the expression levels of the four engineered SAS-6s were mildly elevated compared with that of SAS-6 in the wild type (Fig 5A). Immunofluorescence microscopy using anti-HA antibody showed that the engineered SAS-6s were correctly localized to the centrioles as was wild type SAS-6 (Fig. 6).

To assess the function of the engineered SAS-6s in centriole assembly, the percentage of flagellated cells in each strain was measured (Fig 7), because flagella formation is thought to reflect the presence of centrioles in *Chlamydomonas*. I found that, while ~90% *bld12* cells lacked flagella, ~87% were flagellated in *bld12* cells that expressed wild type SAS-6. Expression of the engineered SAS-6s also rescued the *bld12* phenotype and led to the assembly of functional centrioles to significant degrees, although less effectively than the expression of wild-type SAS-6.

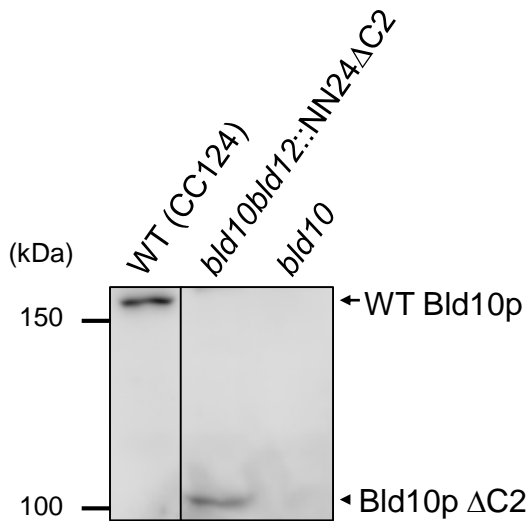
These results suggest that each engineered SAS-6 functions in centriole assembly as a component of the centriole.

Effects of engineered SAS-6s on the 9-fold symmetrical structure of the centriole
Nucleo-flagellar apparatus (NFAp), a cytoskeletal complex containing a nucleus, two mature centrioles, two immature centrioles, and two flagella extending from

A



B



C

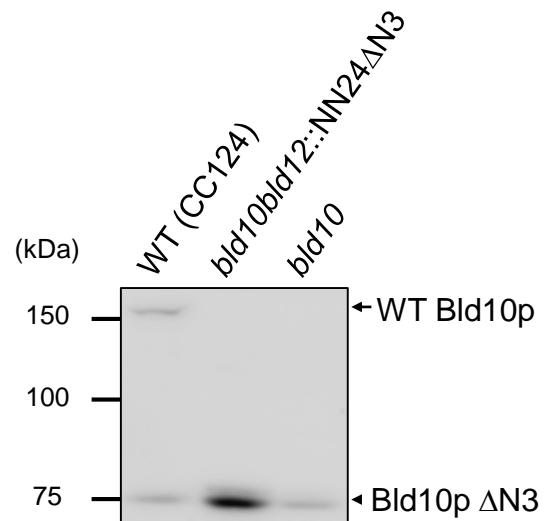


Figure 5. Expression levels of engineered SAS-6s and truncated Bld10ps

(A) Western blot analyses of whole-cell lysates from wild type (WT, CC124), *bld12*, *bld12::SAS-6*, *bld12::NN2*, *bld12::NN15*, *bld12::NN24*, *bld10bld12::NN24ΔC2*, *bld10bld12::NN24ΔN3*, and *bld12::NN26*, using antibodies against SAS-6 (upper blots) and HA (lower blot). The apparent molecular weight of SAS-6 variants is slightly larger than that of endogenous SAS-6 because of the hemagglutinin (HA) tag fused at its C-terminus. (B, C) Western-blot analyses of the whole-cell lysate from CC124, *bld10bld12::NN24ΔC2*, *bld10bld12::NN24ΔN3*, and *bld10* using antibodies against the N-terminal 120 residues of Bld10p (B) or the C-terminal one-third of Bld10p (C). The bands at ~75 kDa that appear in the lanes of CC124 and *bld10* in the right panel are non-specific. These bands overlap with the ΔN3 band.

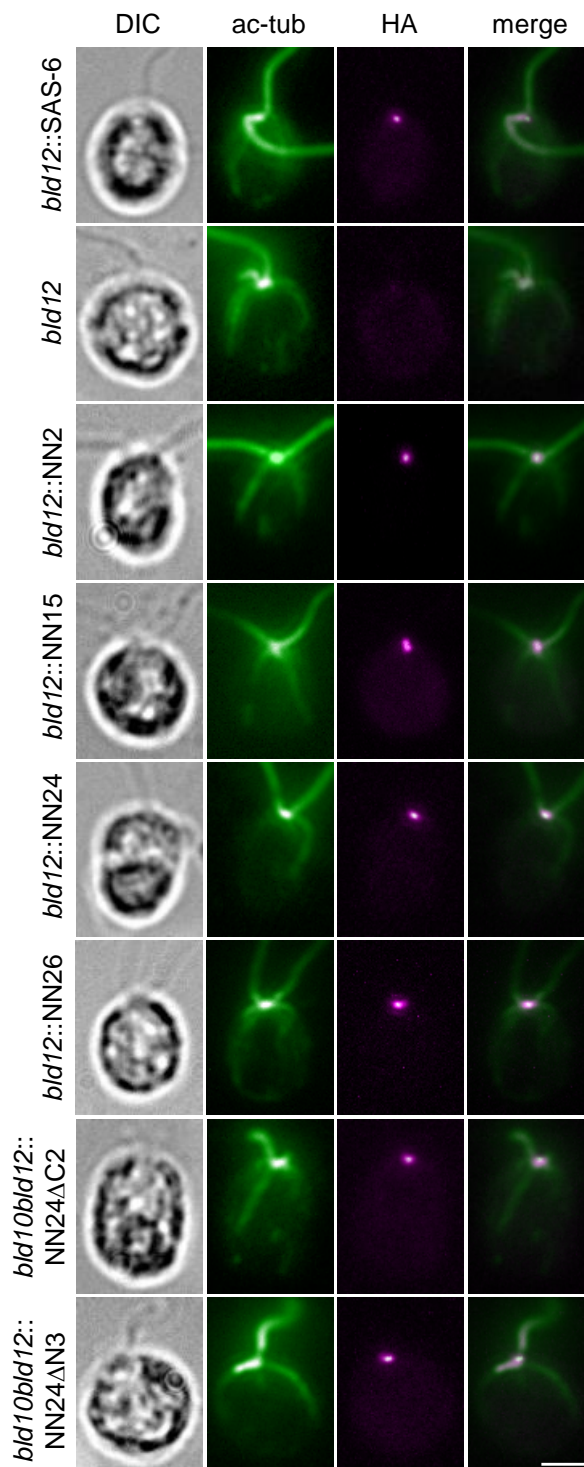


Figure 6. Engineered SAS-6s are localized to centrioles

Indirect immunofluorescence of *bld12::SAS-6*, *bld12*, *bld12::NN2*, *bld12::NN15*, *bld12::NN24*, *bld12::NN26*, *bld10bld12::NN24ΔC2*, and *bld10bld12::NN24ΔN3* cells using antibodies against acetylated α -tubulin (ac-tub, green) and HA (magenta). Left-most panels show differential interference images (DIC). At least 16 cells were observed for each strain, and representative images are shown. Scale bar, 5 μ m.

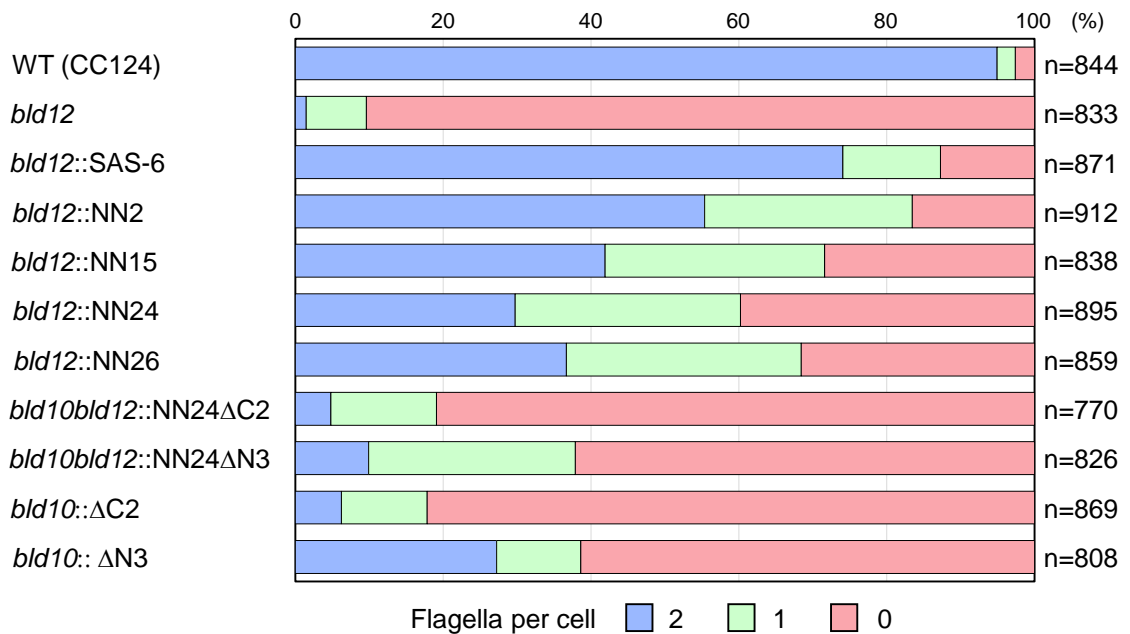


Figure 7. Engineered SAS-6s promote flagellar formation

Percentages of flagellated wild type (CC124), *bld12*, *bld12::SAS-6*, *bld12::NN2*, *bld12::NN15*, *bld12::NN24*, *bld12::NN26*, *bld10bld12::NN24ΔC2*, *bld10bld12::NN24ΔN3*, *bld10::ΔC2* and *bld10::ΔN3* cells. Cells with two (light blue), one (light green), and zero (pink) flagella were counted. n, number of cells counted.

the mature centrioles, was isolated from cells expressing the engineered SAS-6s. The centriole structures in NFAP were observed by transmission electron microscopy. As reported previously, centrioles in the *bld12* NFAP have 7-, 8-, 10-, or 11-fold symmetrical structures, in addition to the normal 9-fold symmetrical one (Fig. 8; Nakazawa et al. 2007). This triplet-number aberration was completely rescued in the transformants expressing the wild-type SAS-6; all the centrioles in the NFAP from the cells had 9 triplets (Fig. 8). In contrast to the expectation from the in vitro results, centrioles from the transformants expressing NN2, NN15, or NN26 cells, which preferentially assembles into cartwheel-like structures with 8-fold symmetry in vitro, still had 9 triplets in most cases (Fig. 8B). However, transformants expressing NN24, which preferentially assembles into structures with 6-fold symmetry in vitro, frequently produced 8-triplet centrioles in addition to the normal 9-triplet centrioles (Fig. 8B). This difference in phenotype observed with the transformant expressing NN24 cannot be solely attributed to an increase of stability in the interaction between the N-terminal domains, because the Kd value of NN24 is similar to that of NN26, of which expression causes only a slight change in centriole structure (Table 1, Fig. 8B).

Effects of NN24 on the cartwheel structure

Expression of SAS-6-NN24 in *Chlamydomonas* cells produced 9- or 8-triplet centrioles (Fig. 8), but not 5-, 6-, or 7-triplet centrioles that would be expected to form if the triplet number were solely determined by the in vitro assembly properties of SAS-6 (Table 1, Fig. 4). To obtain clues to the reason for the discrepancies between in vivo and in vitro effects of the NN24 mutation, the

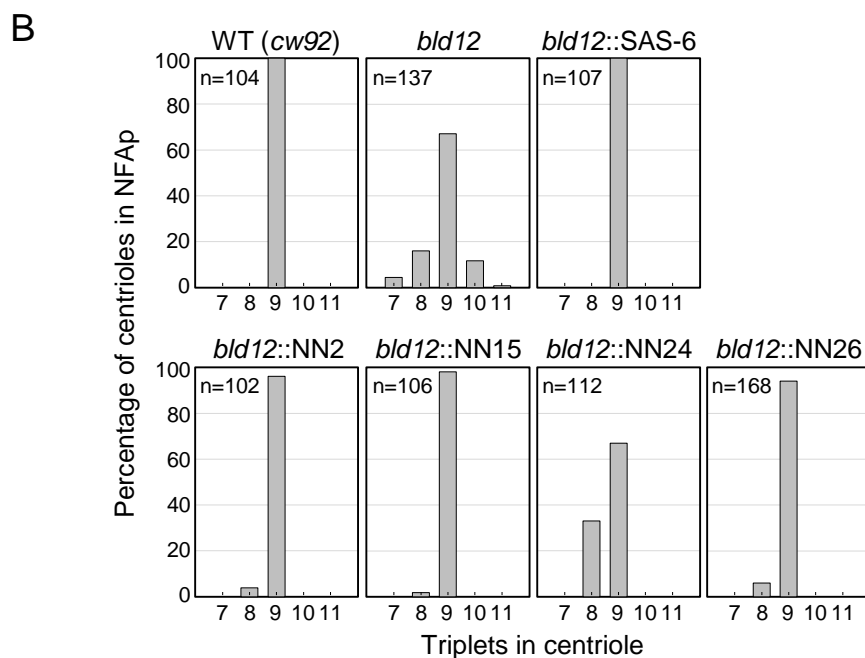
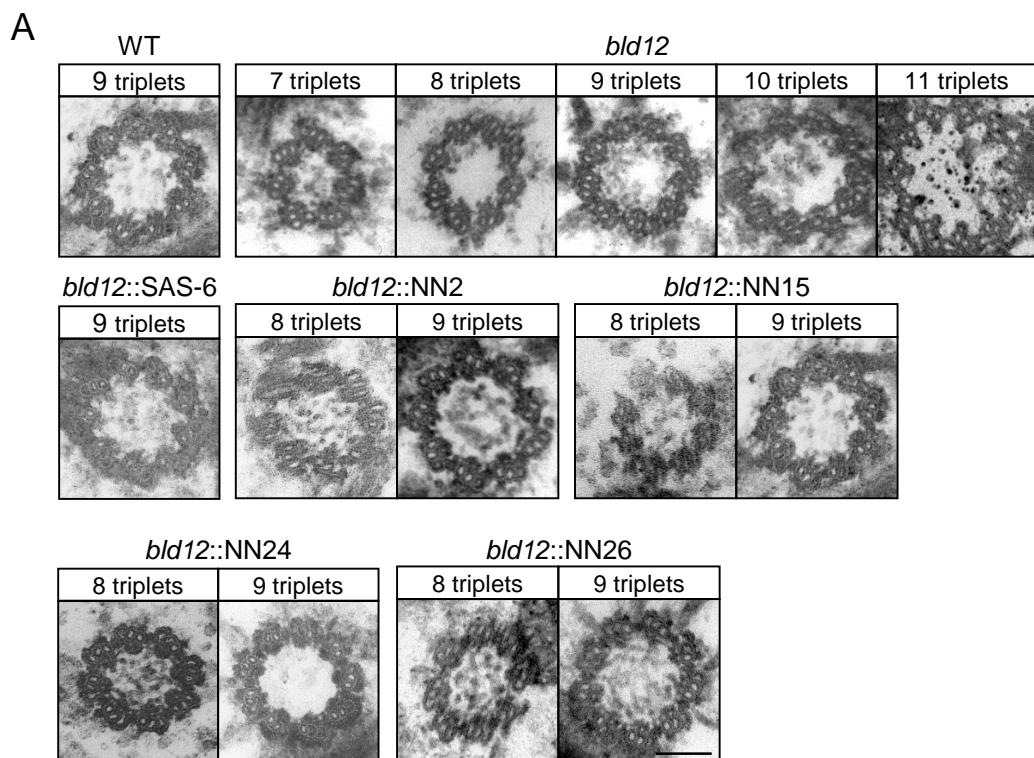


Figure 8. Centriole structures in cells expressing engineered SAS-6s
 (A) Cross-section electron micrographs of wild-type (WT), *bld12*, *bld12::SAS-6*, *bld12::NN2*, *bld12::NN15*, *bld12::NN24* and *bld12::NN26* centrioles. (B) Microtubule triplet-number distributions of centrioles in NFAP preparations from the wild type (WT), *bld12*, *bld12::SAS-6*, *bld12::NN2*, *bld12::NN15*, *bld12::NN24* and *bld12::NN26* cells. n, number of centrioles observed. Scale bar, 100 nm.

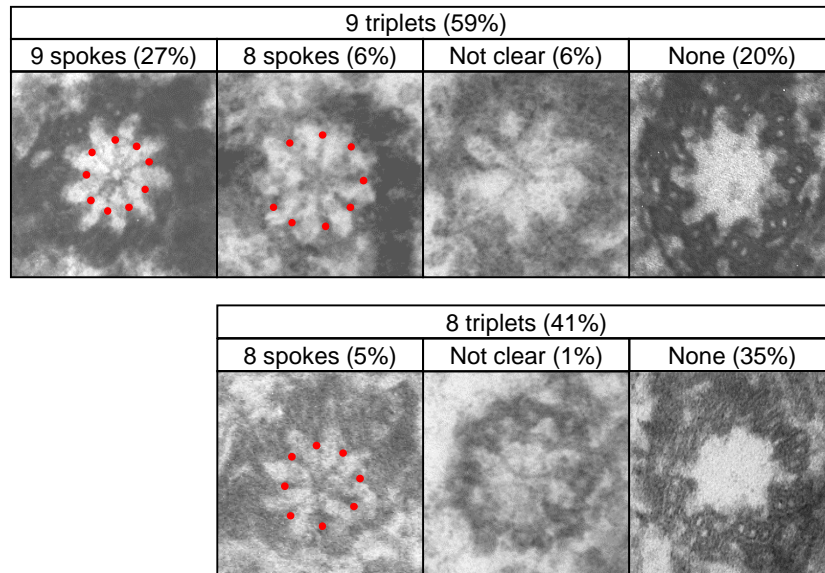
number of cartwheel spokes in the proximal portions of NN24 centrioles was examined by electron microscopy. Unexpectedly, we found that 34% of 9-triplet centrioles and 86% of 8-triplet centrioles lacked cartwheels (Fig. 9A), even though the proximal region of *Chlamydomonas* centrioles normally contain cartwheels (Cavalier-Smith 1974). This is in contrast to centrioles in *bld12*:SAS-6 cells, 87% of which were shown to retain cartwheels in the proximal portion (Fig. 9B). Most interestingly, the cartwheels retained in 9-triplet centrioles had 9 spokes, and those retained in 8-triplet centrioles had 8 spokes (Fig. 9A). These observations indicate that NN24 assembles into a 9- or 8-fold symmetrical structure, which was not observed in vitro. It is likely that additional factor(s) contribute to the symmetry of the cartwheel and centriole in vivo (Fig. 10A).

SAS-6-NN24 combined with Truncated Bld10p forms 6-spoke cartwheels in vivo

Observation of centriole structures in *bld12* suggests that one of the additional factors may be the steric effect of triplet microtubule wall surrounding the cartwheel because 9-triplet centrioles can be assembled even in the absence of SAS-6 (Fig. 8B; Nakazawa et al. 2007). To test this hypothesis, I examined the effect of truncation of Bld10p, which contributes to the length of the spoke and also the strength of microtubule-spoke connection (Fig. 10B). Hiraki et al., (2007) showed that expression of truncated Bld10p missing the N-terminal 54% (denoted $\Delta N3$) or the C-terminal 35% (denoted $\Delta C2$) in *bld10*, a *Chlamydomonas* mutant that totally lacks the *BLD10* gene, causes partial detachment of the cartwheel spoke from triplet microtubules (Fig. 10C-E; Hiraki et al. 2007). Thus I expected that Bld10p truncation will decrease the influence from outer triplets, and possibly show the properties of SAS-6-NN24 tending to form cartwheels with

A

CrNN24 (proximal ends, n=104)



B

bld12::SAS-6 proximal ends (n=37)

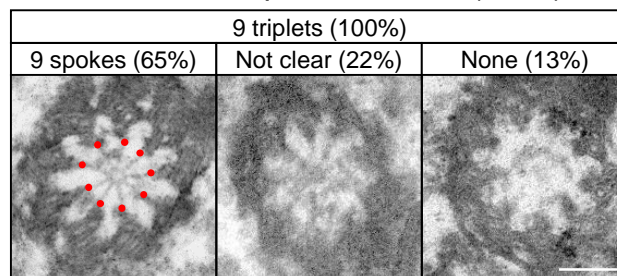
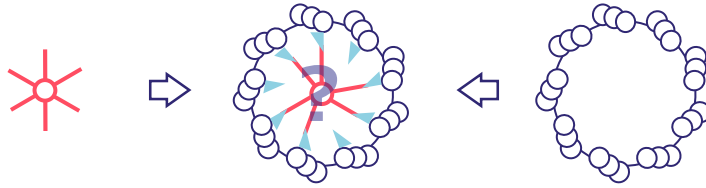


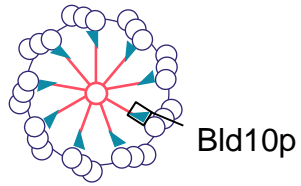
Figure 9. Cartwheel structures in *bld12::NN24* and *bld12::SAS-6* cells

Cross-section electron micrographs of proximal ends of centrioles of *bld12::NN24* (A) and *bld12::SAS-6* (B). Images of 9- and 8-triplet centrioles were classified into four groups: those containing cartwheels with 9 spokes, 8 spokes, cartwheels with an unclear number of spokes (Not clear), and no detectable cartwheels (None). Percentages of centrioles obtained by EM in these classes are indicated in parentheses. Spokes are highlighted with red dots. n, number of centrioles analyzed by EM. Scale bars, 100 nm.

A

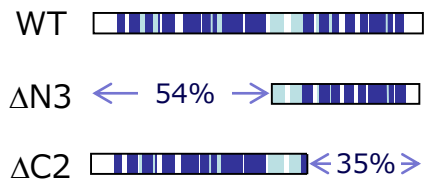


B



Bld10p

C



D

ΔN3 proximal ends (n=45)

9 triplets (100%)		
9 spokes (24%)	Not clear (29%)	None (47%)

E

ΔC2 proximal ends (n=40)

9 triplets (92%)			8 triplets (8%)
9 spokes (25%)	Not clear (32%)	None (35%)	None (8%)

F

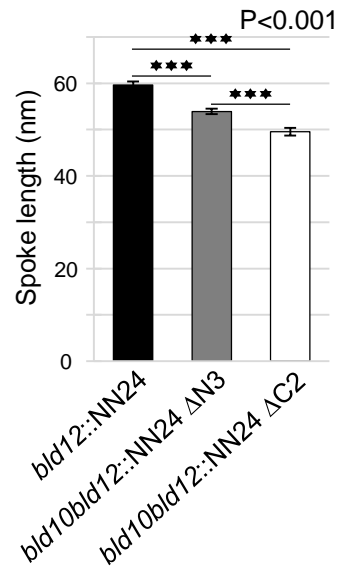


Figure 10. Expression of truncated Bld10ps weakens the interaction between the cartwheel spokes and the microtubules and shortens cartwheel spoke lengths

(A) Schematic diagrams showing the relationship between the cartwheel and the microtubule wall. (B) Schematic diagrams of the cartwheel. Bld10p is localized at the tip of each spoke. (C) Schematic diagrams of full-length and truncated Bld10p. Regions predicted to have high (>80%) and modest (>50%) probabilities of forming coiled-coils are shown in dark and light blue, respectively (D, E). Cross-section electron micrographs of the proximal ends of *bld10::ΔN3* (D) and *bld10::ΔC2* centrioles (E). Images of 9- and 8-triplet centrioles were classified into three groups as in Fig. 8. Percentages of centrioles in these classes are indicated in parentheses. Spokes are highlighted with red dots. (Cartwheel spokes are often detached from triplet microtubules as indicated by yellow arrows. Scale bars, 100 nm. (F) Cartwheel-spoke length measured in EM cross-section micrographs (mean ± SE). Spokes in *bld10bld12::NN24ΔN3* (gray) centrioles are ~10% shorter than those of *bld12::NN24* (black) (53.9 ± 0.6 versus 59.6 ± 0.8 , $p = 3.0e-7$), spokes in *bld10bld12::NN24ΔC2* (white) centrioles are ~17% shorter than those of *bld12::NN24* (49.6 ± 0.8 versus 59.6 ± 0.8 , $p = 0.0003$), and spokes in *bld10bld12::NN24ΔC2* are ~8% shorter than those of *bld10bld12::NN24ΔN3* ($p = 0.0001$).

smaller numbers of spokes. Thus, double mutants, *bld10bld12*, expressing NN24 together with Δ C2 or Δ N3 (*bld10bld12::NN24 Δ C2*, *bld10bld12::NN24 Δ N3*), were established.

Both of the two double mutants expressed short Bld10ps and NN24 at almost the wild-type levels (Fig. 5), and the expressed NN24 localized to centrioles (Fig. 6). While all of the *bld10bld12* cells lacked flagella, the percentage of flagellated cells in either strain was almost the same as in *bld10:: Δ N3* and *bld10:: Δ C2* described previously (Fig. 7; Hiraki et al. 2007). These results suggest that NN24 and the two short Bld10ps function in centriole assembly in the double mutants. Observation of centrioles of the two strains by electron microscopy revealed that >90% centrioles had 8 or 9 microtubules and the rest had six or seven microtubules; these distribution patterns are similar to those in *bld10:: Δ N3*, *bld10:: Δ C2*, and *bld12::NN24* (Fig. 11A-C, 12A-C; Hiraki et al. 2007). In *bld10bld12::NN24 Δ C2* cells, 2.5 and 7.6% of 119 centriole images displayed 6- and 7-triplets respectively (Fig. 12AC), although the majority of the centrioles still displayed 8 or 9 triplets.

To examine the cartwheel structures, proximal regions of centrioles in the two strains were observed by electron microscopy. As expected, the spoke lengths were significantly reduced in both strains (Fig. 10F). Strikingly, cartwheels with 6 and 7 spokes, as expected from the self-assembly properties of NN24, were observed in *bld10bld12::NN24 Δ N3* and *bld10bld12::NN24 Δ C2* (Fig. 11D, 12D, Table 2), while all cartwheels had 9 spokes in *bld10:: Δ N3* and *bld10:: Δ C2* (Fig. 10DE). In *bld10bld12::NN24 Δ C2*, cartwheels with 9 spokes were never observed (Fig. 12D, Table 2B). These results suggest that weakness of the connection allows the engineered SAS-6 to form cartwheels that reflect its intrinsic self-

assembly properties, and that its interaction with the microtubule wall affects the symmetry of the cartwheel.

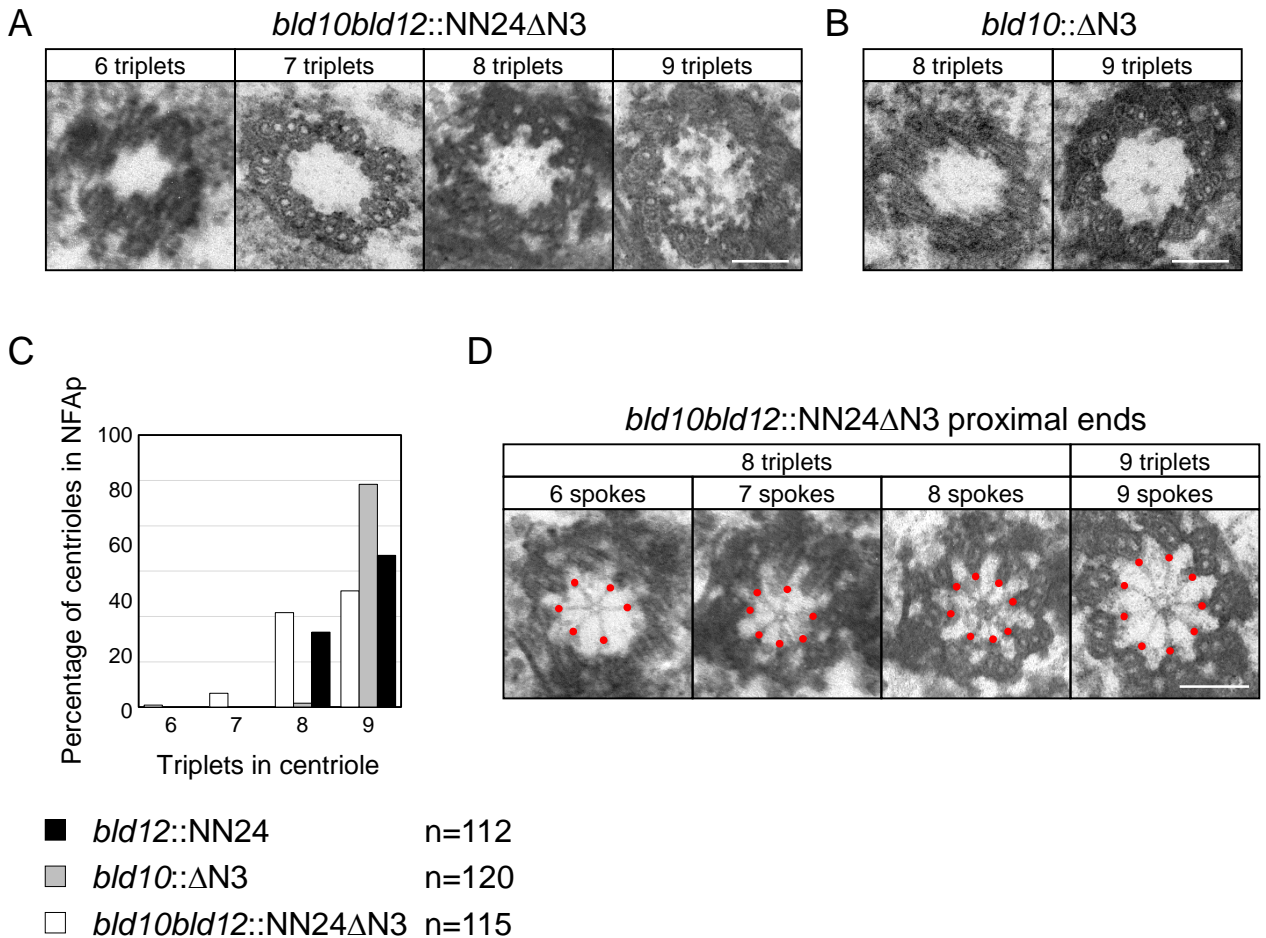


Figure 11. Centriole structures of *bld10bld12::NN24ΔN3*

(A, B) Cross-section electron micrographs of *bld10bld12::NN24ΔN3* (A) and *bld10::ΔN3* centrioles (B). (C) Microtubule triplet-number distributions in *bld12::NN24* (black), *bld10::ΔN3* (gray) and *bld10bld12::NN24ΔN3* (white) centrioles. n, number of centrioles observed. (D) Cross-section electron micrographs of the proximal ends of *bld10bld12::NN24ΔN3* centrioles. Spokes are highlighted with red dots. Scale bars, 100 nm.

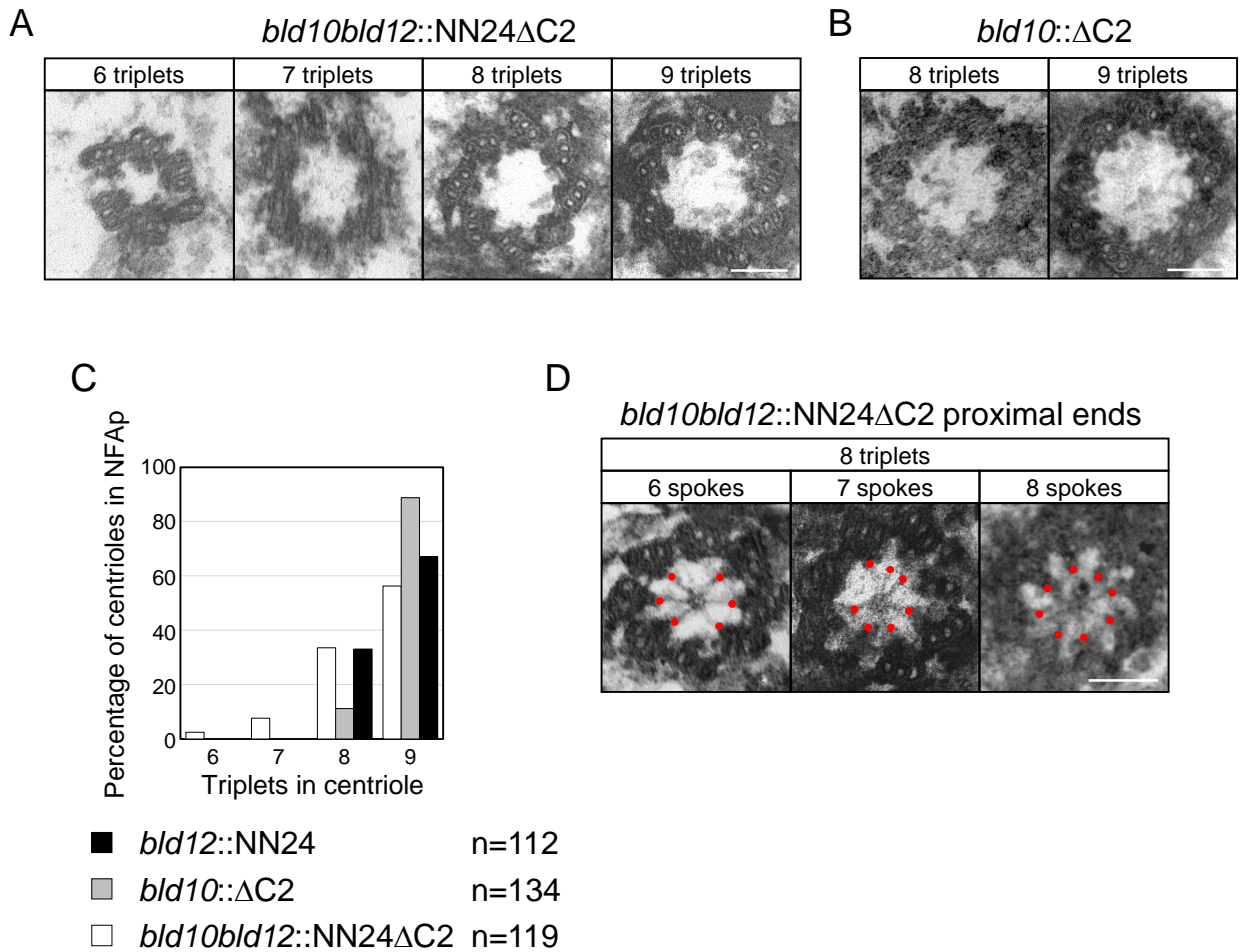


Figure 12. Centriole structures of *bld10bld12::NN24ΔC2*

(A, B) Cross-section electron micrographs of *bld10bld12::NN24ΔC2* (A) and *bld10::ΔC2* (B) centrioles. (C) Microtubule triplet-number distributions in *bld12::NN24* (black), *bld10::ΔC2* (gray) and *bld10bld12::NN24ΔC2* (white) centrioles. n, number of centrioles observed. (D) Cross-section electron micrographs of the proximal ends of *bld10bld12::NN24ΔC2* centrioles. Spokes are highlighted with red dots. Scale bars, 100 nm.

A

bld10bld12::NN24ΔN3 proximal ends (n=76)

		Triplets in centriole			Total
		7	8	9	
Spokes in cartwheel	6	1	2	0	3 (14%)
	7	0	2	0	2 (9 %)
	8	0	6	4	10 (45%)
	9	0	0	7	7 (32%)
Not clear		1	6	11	
No cartwheel		0	14	22	

B

bld10bld12::NN24ΔC2 proximal ends (n=96)

		Triplets in centriole			Total
		7	8	9	
Spokes in cartwheel	6	2	1	1	4 (31%)
	7	0	1	3	4 (31%)
	8	0	1	4	5 (38%)
	9	0	0	0	0 (0 %)
Not clear		1	15	28	
No cartwheel		0	13	26	

Table 2. Distributions of triplet and spoke numbers in centrioles

76 and 96 cross-section electron micrographs of the proximal ends of the centrioles in *bld10bld12::NN24ΔN3* (A) and *bld10bld12::NN24ΔC2* (B) were classified into 18 groups based on their number of triplet microtubules, cartwheel spokes and appearance of the cartwheel. Note that the number of spokes in most cartwheels of *bld10bld12::NN24ΔC2* was less than that of the microtubule triplets.

Discussion

In Part I, I performed experiments to understand the precise role of the cartwheel in centriole assembly. For this purpose, I examined the effect of altered assembly properties of SAS-6 on the centriole structure, as well as the effect of weakened connection between the cartwheel and triplet microtubules on the cartwheel structure.

Limited effects of *in vitro* assembly properties of SAS-6 on the centriole structure

I have shown that expression of NN24, which tends to assemble into a cartwheel-like structure with 6-fold symmetry *in vitro*, indeed reduces the degree of the symmetry of centrioles, although to a lesser extent compared to what was expected from the *in vitro* data. To the best of my knowledge, this result represents the first demonstration that the assembly properties of SAS-6 affect the overall structure of the centriole.

At the same time, however, I have also shown that the centriole structure in the NN24-expressing cells does not faithfully reflect the *in vitro* properties of SAS-6-NN24 (Table 1): 67% centrioles in the cells had 9 triplets and no centrioles displayed 6 or 7 triplets (Figure 8). These results suggest that a mechanism independent of SAS-6 exerts pressure on centriole assembly toward 9-fold symmetry. Although the molecular entity is not yet identified, such a mechanism has been suggested to exist from the analysis of the *Chlamydomonas* mutant *bld12*, which, in the absence of SAS-6, produces 9-triplet centrioles in addition to smaller numbers of 7-, 8-, 10-, and 11-triplet centrioles (Fig. 8; Nakazawa et al. 2007). The stability of the centriole's 9-fold symmetry observed in the NN24-

expressing cells is likely caused by the same SAS-6-independent mechanism.

Steric effects of the triplet microtubule wall on the cartwheel

Surprisingly, this SAS-6-independent mechanism appears to affect the cartwheel structure also, as evidenced by the observation that NN24 in the cell frequently formed 9-spoke cartwheels within 9-triplet centrioles (Figure 9A). There may be some cellular factors that promote the formation of 9-fold symmetrical assembly of SAS-6 even with the NN24 mutation. I surmised that such a factor, if any, is closely related to the triplet microtubules. In fact, with truncation of Bld10p, which tends to destabilize the connection between the cartwheel spoke and the triplet, NN24 produced cartwheels that reflected its *in vitro* tendency to form smaller rings (Table 1). For example, it produced 8- or 9-triplet centrioles, and 6- or 7- spoke cartwheels *in vivo* (Fig. 11D, 12D, Table 2).

Dynamic interaction model for centriole assembly

The finding that the triplet arrangement affects the cartwheel structure is inconsistent with the idea that the cartwheel serves as the template for the triplet assembly (Fig. 13A). Here, I thus propose a new model: circularly arranged microtubules and cartwheels can form independently (and possibly transiently) in the cytoplasm and they undergo dynamic interactions, which result in the stabilization of 9-fold symmetrical centrioles (Figure 13B). When NN24 is expressed, the spoke number of cartwheels may be around 6, while the triplet number must be around 9. This mismatch should cause a decreased efficiency of centriole formation (Fig. 7), and, as a result of the imperfect interaction, 8-triplet centrioles are produced in addition to 9-triplet centrioles

(Fig. 8). In 8-triplet centrioles with NN24, 86% lacked the cartwheel (Figure 9A), probably because the inner space of the 8-triplet centriole is too small to accommodate the cartwheel. The Bld10p truncation allows 8-triplet and even 7-triplet centrioles to retain cartwheels (Fig. 11A-C, 12A-C), because the truncation sufficiently shortens the spoke length to fit in the small-diameter centrioles (Fig. 10F).

A



B

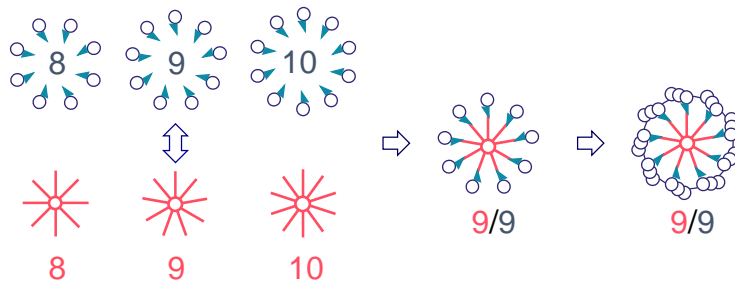


Figure 13. Models of centriole assembly

(A) Scaffold model of centriole assembly. This widely acknowledged model posits that the 9-fold symmetric cartwheel (pink) is formed first and functions as a template for the assembly of the 9-fold symmetric microtubule wall (blue). (B) Interdependence model of centriole assembly. Previous data and the results presented here suggest that both the cartwheel and the microtubule wall can assemble in parallel into transient structures with symmetries ranging predominantly from 8- to 10-fold. The model proposes that the precise match and interplay between a 9-fold symmetric cartwheel and a 9-fold symmetric microtubule wall is essential to produce a stable and native centriole.

第2章

本章については、5年以内に雑誌等で刊行予定のため、非公開。

General discussion

第2章の内容を含むため、非公開。

Acknowledgements

I would like to express my sincere gratitude to my supervisor Dr. Masafumi Hirono (Hosei University) for his encouragement and guidance throughout the course of this study. I am grateful to my supervisor Dr. Yoshitaka Oka (University of Tokyo) for his support, Dr. Ritsu Kamiya (Gakushuin University) for his critical reading of the manuscript, and Takako Kato-Minoura (Chuo University) for letting me use the electron microscope of her department.

I thank Dr. Yuki Nakazawa (Hosei University) for her helpful advice and fruitful discussion. I also thank Dr. Haru-aki Yanagisawa (University of Tokyo) for providing the genomic SAS-6 plasmid. Last but not least, I thank collaborators of the Part I study, especially Drs. Michel O. Steinmetz and Hilbert Manuel (Paul Scherrer Institute), for their friendship and encouragement.

Reference

- Bettencourt-Dias, M., F. Hildebrandt, D. Pellman, G. Woods, and S. A. Godinho. 2011. 'Centrosomes and cilia in human disease', *Trends Genet*, 27: 307-15.
- Bornens, M. 2012. 'The centrosome in cells and organisms', *Science*, 335: 422-6.
- Carvalho-Santos, Z., J. Azimzadeh, J. B. Pereira-Leal, and M. Bettencourt-Dias. 2011. 'Evolution: Tracing the origins of centrioles, cilia, and flagella', *J Cell Biol*, 194: 165-75.
- Cavalier-Smith, T. 1974. 'Basal body and flagellar development during the vegetative cell cycle and the sexual cycle of *Chlamydomonas reinhardtii*', *J Cell Sci*, 16: 529-56.
- Conduit, P. T., A. Wainman, and J. W. Raff. 2015. 'Centrosome function and assembly in animal cells', *Nat Rev Mol Cell Biol*, 16: 611-24.
- de Harven, Etienne, and W. Bernhard. 1956. 'Etude au microscope electronique de l'ultrastructure du centriole chez les vertébrés', *Zeitschrift für Zellforschung und Mikroskopische Anatomie*, 45: 378-98.
- Dippell, R. V. 1968. 'The development of basal bodies in paramecium', *Proceedings of the National Academy of Sciences of the United States of America*, 61: 461-68.
- Fawcett, Don W., and Keith R. Porter. 1954. 'A study of the fine structure of ciliated epithelia', *Journal of Morphology*, 94: 221-81.
- Firat-Karalar, E. N., and T. Stearns. 2014. 'The centriole duplication cycle', *Philos Trans R Soc Lond B Biol Sci*, 369.
- Gonczy, P. 2012. 'Towards a molecular architecture of centriole assembly', *Nat Rev Mol Cell Biol*, 13: 425-35.

- Gorman, D. S., and R. P. Levine. 1965. 'Cytochrome f and plastocyanin: their sequence in the photosynthetic electron transport chain of *Chlamydomonas reinhardtii*', *Proc Natl Acad Sci U S A*, 54: 1665-9.
- Harris, E.H. 1989. 'The *Chlamydomonas* Sourcebook', *San Diego: Academic Press*.
- Hiraki, M. 2007. 'Hiraki doctor report'.
- Hiraki, M., Y. Nakazawa, R. Kamiya, and M. Hirono. 2007. 'Bld10p constitutes the cartwheel-spoke tip and stabilizes the 9-fold symmetry of the centriole', *Curr Biol*, 17: 1778-83.
- Hirono, M. 2014. 'Cartwheel assembly', *Philos Trans R Soc Lond B Biol Sci*, 369.
- Kitagawa, D., I. Vakonakis, N. Olieric, M. Hilbert, D. Keller, V. Olieric, M. Bortfeld, M. C. Erat, I. Fluckiger, P. Gonczy, and M. O. Steinmetz. 2011. 'Structural basis of the 9-fold symmetry of centrioles', *Cell*, 144: 364-75.
- Kraatz, S., P. Guichard, J. M. Obbineni, N. Olieric, G. N. Hatzopoulos, M. Hilbert, I. Sen, J. Missimer, P. Gonczy, and M. O. Steinmetz. 2016. 'The Human Centriolar Protein CEP135 Contains a Two-Stranded Coiled-Coil Domain Critical for Microtubule Binding', *Structure*, 24: 1358-71.
- Kuriyama, R., and G. G. Borisy. 1981. 'Centriole cycle in Chinese hamster ovary cells as determined by whole-mount electron microscopy', *J Cell Biol*, 91: 814-21.
- Loncarek, J., and M. Bettencourt-Dias. 2017. 'Building the right centriole for each cell type', *J Cell Biol*.
- Matsuura, Kumi, Paul A. Lefebvre, Ritsu Kamiya, and Masafumi Hirono. 2004. 'Bld10p, a novel protein essential for basal body assembly in *Chlamydomonas*', *The Journal of Cell Biology*, 165: 663-71.

- McNitt, R. 1974. 'Centriole ultrastructure and its possible role in microtubule formation in an aquatic fungus', *Protoplasma*, 80: 91-108.
- Nakazawa, Y., M. Hiraki, R. Kamiya, and M. Hirono. 2007. 'SAS-6 is a cartwheel protein that establishes the 9-fold symmetry of the centriole', *Curr Biol*, 17: 2169-74.
- Nigg, E. A., and J. W. Raff. 2009. 'Centrioles, centrosomes, and cilia in health and disease', *Cell*, 139: 663-78.
- Olieric, Natacha, Melanie Kuchen, Sandro Wagen, Marion Sauter, Stephanie Crone, Sonia Edmondson, Daniel Frey, Christian Ostermeier, Michel O. Steinmetz, and Rolf Jaussi. 2010. 'Automated seamless DNA co-transformation cloning with direct expression vectors applying positive or negative insert selection', *BMC Biotechnology*, 10: 56.
- Pfreundschuh, Moritz, David Alsteens, Manuel Hilbert, Michel O. Steinmetz, and Daniel J. Müller. 2014. 'Localizing Chemical Groups while Imaging Single Native Proteins by High-Resolution Atomic Force Microscopy', *Nano Letters*, 14: 2957-64.
- Shimogawara, K., S. Fujiwara, A. Grossman, and H. Usuda. 1998. 'High-efficiency transformation of *Chlamydomonas reinhardtii* by electroporation', *Genetics*, 148: 1821-8.
- Silflow, C. D., M. LaVoie, L. W. Tam, S. Tousey, M. Sanders, W. Wu, M. Borodovsky, and P. A. Lefebvre. 2001. 'The Vfl1 Protein in *Chlamydomonas* localizes in a rotationally asymmetric pattern at the distal ends of the basal bodies', *J Cell Biol*, 153: 63-74.
- Sizova, I., M. Fuhrmann, and P. Hegemann. 2001. 'A *Streptomyces rimosus* aphVIII gene coding for a new type phosphotransferase provides stable

- antibiotic resistance to *Chlamydomonas reinhardtii*', *Gene*, 277: 221-9.
- van Breugel, M., M. Hirono, A. Andreeva, H. A. Yanagisawa, S. Yamaguchi, Y. Nakazawa, N. Morgner, M. Petrovich, I. O. Ebong, C. V. Robinson, C. M. Johnson, D. Veprintsev, and B. Zuber. 2011. 'Structures of SAS-6 suggest its organization in centrioles', *Science*, 331: 1196-9.
- Winey, M., and E. O'Toole. 2014. 'Centriole structure', *Philos Trans R Soc Lond B Biol Sci*, 369.
- Wright, R. L., J. Salisbury, and J. W. Jarvik. 1985. 'A nucleus-basal body connector in *Chlamydomonas reinhardtii* that may function in basal body localization or segregation', *J Cell Biol*, 101: 1903-12.